Peer-reviewed version available at Energies 2017, 10, 949; doi:10.3390/en10070949

Article

Tracking Control with Zero Phase-difference for Linear Switched Reluctance Machines Network

Bo Zhang[1,2], J.F. Pan[1],Jianping Yuan[2,*], Wufeng Rao[1,2], Li Qiu[1], Jianjun Luo[2] and Honghua Dai[2]

[1] College of Mechatronics and Control Engineering, Shenzhen University, Shenzhen,518060, China; zhangbo@szu.edu.cn(B.Z.);pjf@szu.edu.cn(J.F.P.);michaelmile@qq.com(W.R.);qiuli@szu.edu.cn;

[2] Laboratory of Advanced Unmanned Systems Technology, Northwestern Polytechnical University, Shenzhen,518060, China;jjluo@nwpu.edu.cn(J.L);hhdai@nwpu.edu.cn

* Correspondence: jianpingyuan@yeah.net; Tel.: +86-755-2653-1066

Abstract: This paper discusses about control of the linear switched reluctance machines (LSRMs) network for the zero phase-difference tracking to a sinusoidal reference. The dynamics of each LSRM is derived by online system identification and modeled as a second-order linear system. Accordingly, based on the coupled harmonic oscillators synchronization manner, a distributed control is proposed to synchronize each LSRM state to a virtual LSRM node representing the external sinusoidal reference for tracking it with zero phase-difference. Subsequently, a simulation scenario and an experimental platform with the identical parameter setup are designed to investigate the tracking performance of the LSRMs network constructed by the proposed distributed control. Finally, the simulation and experimental results verify the effectiveness of the proposed LSRMs network controller, and also prove that the coupled harmonic oscillators synchronization method can improve the synchronization tracking performance and precision.

Keywords: linear switched reluctance machine (LSRM); coordinated network; distributed control; synchronization tracking

1. Introduction

Linear tracking control systems based on direct drive linear machines are vastly used in manufacture industry, such as parts assembly, printed circuit boarding (PCB) drilling and chip processing, etc. In addition, there are many tasks that require a cooperation of many linear machines to work harmonically. For example, in a multi-station PCB drilling machine, each linear machine acts as one working unit. The board being processed requires the linear machines to track the command position precisely and coordinates with each other to finish the whole drilling work. Therefore, each linear machine often demands the state information from other machines, so as to work cooperatively and synchronously. The overall motion control performance can be improved such as faster operation time, more efficiency and the annihilation of accumulated errors, etc., compared to a traditional sequenced working manner [1]. Furthermore, if multiple linear machines can be organized as a coordinated and distributed motion tracking network and each machine has the position controller, sensor and driver of its own, the ultimate global tracking control goal can be emerged by local communications among the independent linear machine nodes with local controllers, without the necessity of any global supervision or decision [2].

Among different types of linear machines, a linear switched reluctance motor (LSRM) has the advantages of a simple and robust mechanical structure, low cost, high reliability and free of frequent maintenance or adjustments [3]. Current motion tracking research on LSRMs mainly focuses on the control performance improvement for single machine based position control systems [4–7]. In [4], an

adaptive position controller is inspected to compensate uncertain behaviors of a double-sided LSRM. A nonlinear proportional differential (PD) tracking controller based on the tracking differentiator is proposed for a real-time LSRM suspension system, to achieve a better dynamic position response [5]. A sliding mode position control technique is investigated in [6] and a passivity-based control algorithm is proposed for the LSRM position tracking system to overcome the inherent nonlinear characteristics and ameliorate system robustness against uncertainties and bounded disturbances [7]. From the latest development on the tracking control performance of LSRMs, the ratio of an absolute dynamic tracking error to full range of 5‰ can be achieved in single LSRM position control applications.

As remarked above, by employing a multi-agent network formed by distributed control on the same product line, all LSRMs can be coordinated to work together harmonically. Up till now, the experiment and technique studies on the tracking control network based on LSRMs have gained much attention, and related researches are increasing [8], [9]. Current analysis of motion coordinated control of multi-agent network mainly focuses on distributed control methods with multi-agent network [10–16], which provides a guidance to the LSRMs network. Ref. [10] primarily investigates the consensus for coordinated control of multi-agent networks, and establishes the connections between structural properties and the performance of networks. Cao [11] elaborates the main results and the progress about coordinated control algorithms for multi-agent networks and summarizes the future directions of the distributed coordination of multi-agent. At present, multi-agent network study has been classified into several major aspects, which include constrained or imperfect communication [12], delay or switching information linkage [13], [14], agent with nonlinear dynamics [15], influence of noise [16], etc. Furthermore, the multi-agent network by distributed control distributed control algorithms have been exploited in the regime of spacecraft cluster [17], robots coordination [18], and unmanned aerial vehicle formation [19].

It can be concluded from the above analysis that current theoretical work mainly concentrates on distributed control methods to achieve the network synchronization under some network topology constraint condition. The ultimate goal is to form a stable synchronized motion among the multiple agents within the network employing distributed and networked control algorithms. But in most industry processes, multiple LSRMs as a multi-agent network is not only required to motion synchronization but also to track some specific desired trajectory [20]. In practice, directly control every agent in a multi-agent network with a number of agents might be impossible or unnecessary. Therefore, pinning control is regarded as a desirable method [21]. Accordingly, the multi-agent network formed by the pinning control is defined as the leader-following network [2]. In leader-following network, a reference can be accessed directly by minority agents named as leaders only, and then the rest of agents named as followers are steered to implement the synchronized motion to the common reference by the effect of the distributed control. Wang [22] reviews elaborately advances in pinning control approaches, including the feasibility, stability and effectiveness of pinning control and pinning-based consensus and flocking control of mobile multi-agent networked systems. One of the challenges with leader-following network is that the reference possesses different dynamic characteristics from all agents. Cao [23] proposes a distributed consensus tracking algorithm for second-order dynamics guarantees global exponential tracking without acceleration measurements, and the dynamic reference is modeled as the virtual leader with time-varying velocity. Especially, in industrial processes, for implementing much of repetitive work, some periodic motion modes such as sinusoid always are as the desired motion . Wang [24] proposes an internal model controller compensating the reference dynamics for output synchronization of more general heterogeneous multi-agents systems. Wieland [25] proves that an internal model principle is necessary and sufficient for exponential synchronizability of the group to some common, non-trivial output trajectory, bounded by a polynomial function in time, and also notes that the internal model components may give rise to the instability of the multi-agent network under the influence of parametric uncertainties.

In this paper, the mathematical model of each LSRM is derived by the online system identification , which is essential modeled as a general second-order linear system. Second, inspired by coupled harmonic oscillators [26], [27], a distributed control is designed to track a sinusoidal reference with zero phase-difference among each LSRM and the reference as virtual node , so as to improve the tracking performance of the LSRMs network. Last, simulation and experimental verification is provided to prove the effectiveness of the network controller design scheme.

The main contributions of this paper are three folds. First, for the convenience of the coordinated motion control, the reference signal is modeled as a virtual LSRM node which has the same dynamic characteristics as three moter nodes based on the proposed distributed tracking control strategy. Second, three motor nodes and the virtual node can be realized the synchronization control by adopting the coupled harmonic oscillators method, so as to achieve for tracking the sinusoidal reference signal with zero phase-difference. Finally, the distributed tracking control performance for the LSRMs network is investigated by a simulation and experimental platform testing.

2. Model and Preliminaries

2.1. Mathematical Preliminaries

Notations: Let $\mathbb{R}^n$ and $\mathbb{R}^{n\times m}$ indicate the n dimensional Euclidean space and the set of $n \times m$ real matrices, respectively. I_N represents a N-dimension unit matrix. The Kronecker product of matrices $A \in \mathbb{R}^{n\times m}$ and $B \in \mathbb{R}^{p\times q}$ satisfies the following properties as,

$$\begin{aligned}(A \otimes B)(C \otimes D) &= AC \otimes BD \\ (A \otimes B)^T &= A^T \otimes B^T \\ k(A \otimes B) &= (kA) \otimes B = A \otimes (kB) \\ A \otimes (B_1 + B_2) &= A \otimes B_1 + A \otimes B_2\end{aligned} \tag{1}$$

The interaction topology of coordinated network building LSRMs network system is represented using a directed graph $\mathcal{G} = (\mathcal{V}, \mathcal{E})$, as shown in Fig. 1, which is characterized by an edge-linked node set $\mathcal{V}$. It denotes N local closed-loop LSRM systems termed as LSRM node $L_i, i = 1, \ldots, N$, formed by each LSRM and its local controller individually. An edge set $\mathcal{E} \in \mathcal{V} \times \mathcal{V}$ represents M communication linkages among all LSRM nodes, where an edge exists from LSRM node L_j to L_i if $(j, i) \in \mathcal{E}$. If a set composed of LSRM nodes L_j satisfies $(j, i) \in \mathcal{E}$, it is named as the neighbor set $\mathcal{N}_i$ associated with the LSRM node L_i. A directed graph contains a directed spanning tree if there exists a node called root such that there is one or more than one directed path from this node to every other node, such as L_1 in Fig. 1. A path from v_1 to v_k in $\mathcal{G}$ is formed by the $\mathcal{E}$ subset $\{(v_i, v_i + 1)|i = 1, \ldots, k - 1)\}$. $\mathcal{A}, \mathcal{L}$ denote its adjacency matrix and Laplacian matrix of $\mathcal{G}$, respectively.

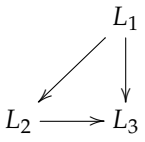

Figure 1. Topology of coodinated network

2.2. Model of the LSRM node

Any of the N three-phase LSRMs (indexed as i-th, $i = 1, \ldots, N$) can be described in the voltage equation as [4],

$$u_{k,i} = R_{k,i} i_{k,i} + \frac{d\lambda_{k,i}}{dt}, k = a, b, c \tag{2}$$

where $u_{k,i}$, $R_{k,i}$ and $i_{k,i}$ are terminal voltage, coil resistance and current, respectively. $\lambda_{k,i}$ represents the flux-linkage of the k-th winding. Each LSRM can also be depicted as the second-order dynamics as follows,

$$m_i \frac{d^2 x_i}{dt^2} + B_i \frac{dx_i}{dt} + fl_i = f_i \tag{3}$$

where x_i, B_i, m_i, f_i and fl_i represent position, friction coefficient, mass, total and load force of the i-th LSRM, respectively. The second-order system as Eq. (3) can be further represented in the discrete-time form as [5],

$$A(z^{-1}) x_i = B(z^{-1}) f_i + e_i \tag{4}$$

where $A(z^{-1})$ and $B(z^{-1})$ are polynomials to be determined, z is the discrete-time operator, and e_i denotes unknown disturbances of the i-th LSRM.The polynomials $A(z^{-1})$ and $B(z^{-1})$ correspond to the typical discrete-time form are depicted as,

$$\begin{cases} A(z^{-1}) = 1 + a_1 z^{-1} + a_2 z^{-2} \\ B(z^{-1}) = b_0 + b_1 z^{-1} \end{cases} \tag{5}$$

The purpose of online system identification is to correctly estimate a_1, a_2, b_0 and b_1 that contain all dynamic information of each LSRM. For the n-th estimation, Eq. (4) can also be considered as a typical least square form as follows,

$$x_i(k) = \varphi^T(k-1)\theta + e_i(k) \tag{6}$$

where $x_i(k)$ is the i-th LSRM state including the position and velocity at time step k, and

$$\begin{cases} \theta = \begin{bmatrix} a_1 & a_2 & b_0 & b_1 \end{bmatrix}^T \\ \varphi(k-1) = \begin{bmatrix} -x_i(k-1) \cdots -x_i(k-n) f_i(k) \cdots f_i(k-n) \end{bmatrix}^T \end{cases} \tag{7}$$

The parameters described in Eq. (7) can be estimated by the recursive least square method as [29],

$$\begin{cases} \hat{\theta}(k) = \hat{\theta}(k-1) + R(k) e_i(k) \\ R(k) = P(k-1)\varphi(k-1)\left[\rho + \varphi^T(k) P(k-1) \varphi(k)\right]^{-1} \\ P(k) = \rho^{-1}\left[I - K(k)\varphi^T(k)\right] P(k-1) \end{cases} \tag{8}$$

where P is the covariance matrix and R is the gain, K and I are respectively the gain matrix and an identity matrix with compatible dimensions, and $\hat{\theta}$ represents the estimated value of θ through the identification processc. ρ is the forgetting factor that reflects the relationship between the converging rate and tracking ability and it falls into 0 and 1. For the LSRM, ρ is chosen as 0.98 for moderate converging ripples and a fast identification speed. For initial values, $P(0)$ can be chosen as $\eta \cdot I_4$ with η as a constant value of 50. Stochastic errors e_i can be represented as,

$$e_i(k) = x_i(k) - \varphi^T(k)\hat{\theta}(k-1) \tag{9}$$

Preprints (www.preprints.org) | NOT PEER-REVIEWED | Posted: 25 May 2017 doi:10.20944/preprints201705.0181.v1

Peer-reviewed version available at Energies 2017, 10, 949; doi:10.3390/en10070949

If the relative error from the present to the last step is comparatively a small positive value ζ, it can be regarded that the present estimated value is correct. Then the termination criterion can be represented as,

$$\left| \frac{\hat{\theta}(k+1) - \hat{\theta}(k)}{\hat{\theta}(k)} \right| < \zeta \tag{10}$$

Any local LSRM control system is defined as a LSRM node in the LSRMs network. The control block diagram for any LSRM node can be depicted as shown in Fig. 2. The LSRM node L_i receives both the position feedback information from its linear encoder and the node L_j, and only the leader node (i.e. the node located at the root of a certain spanning tree in a coordinated network topology) accesses the external reference information, i.e the input signal of the LSRMs network from outside. Each LSRM node is composed of a local position controller, the multiphase excitation scheme with look-up table linearizion, current controllers and a LSRM, and the control scheme conforms to the typical dual-loop architecture [28]. For the LSRM node L_i, position error is decided from the difference between reference (the leader only) and actual position ρ_i of the i-th LSRM, along with the position information ρ_j from the LSRM node L_j. The position controller then calculates the control input, and the multi-phase excitation with the look-up table linearizion scheme determines the current command for the k-th phase of the i-th LSRM, according to the current position of the i-th LSRM. Then the current controller outputs the actual current to the k-th winding.

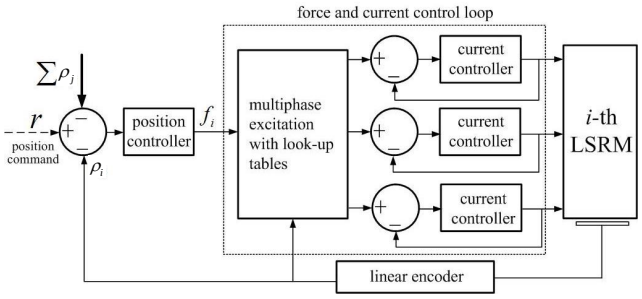

Figure 2. Control block diagram for the LSRM node.

Rearranging Eq. (3) in the state-space form, we have

$$\begin{bmatrix} \dot{\rho}_i \\ \ddot{\rho}_i \end{bmatrix} = \begin{bmatrix} 0 & 1 \\ 0 & -\frac{B_i}{m_i} \end{bmatrix} \begin{bmatrix} \rho_i \\ \dot{\rho}_i \end{bmatrix} + \begin{bmatrix} 0 \\ \frac{1}{m_i} \end{bmatrix} u_i \tag{11}$$

where $u_i = f_i - fl_i$ is the control input of the i-th LSRM.

3. Synchronization Tracking Control Design

Since each LSRM is a mechatronic device fulfilling double-acting periodic line motion, some sinusoidal or its combinatorial patterns are often applied as the predefined trajectory planning some desired reciprocating motion for the LSRMs network. For this purpose, inspired by coupled harmonic oscillators synchronization proposed in [26], [27], the distributed control law can be formulated as,

$$u_i = -\alpha\rho_i + B_i\dot{\rho}_i - \sum_{j\in\mathcal{N}_i} K_{d,i}\left[\dot{\rho}_i(t) - \dot{\rho}_j(t)\right] \tag{12}$$

where α is a parameter assciated with the angular frequency ω of the reference sinusoidal signal. Substituting Eq. (12) into Eq. (11) , the LSRM node L_i can be depicted as,

$$\begin{bmatrix} \dot{\rho}_i \\ \ddot{\rho}_i \end{bmatrix} = \left\{ \begin{bmatrix} 0 & 1 \\ 0 & -\frac{B_i}{m_i} \end{bmatrix} + \begin{bmatrix} 0 & 0 \\ -\frac{\alpha}{m_i} & \frac{B_i}{m_i} \end{bmatrix} \right\} \begin{bmatrix} \rho_i \\ \dot{\rho}_i \end{bmatrix} - \sum_{j\in\mathcal{N}_i} \begin{bmatrix} 0 \\ \frac{K_{d,i}}{m_i} \end{bmatrix} \begin{bmatrix} \dot{\rho}_i(t) - \dot{\rho}_j(t) \end{bmatrix}$$

$$= \begin{bmatrix} 0 & 1 \\ -\frac{\alpha}{m_i} & 0 \end{bmatrix} \begin{bmatrix} \rho_i \\ \dot{\rho}_i \end{bmatrix} - \sum_{j \in \mathcal{N}_i} \begin{bmatrix} 0 \\ \frac{K_{d,i}}{m_i} \end{bmatrix} \begin{bmatrix} \dot{\rho}_i(t) - \dot{\rho}_j(t) \end{bmatrix} \tag{13}$$

Let $\omega^2 = \frac{\alpha}{m_i}$, $k_b = \frac{K_{d,i}}{m_i}$, $\rho = [\rho_1, \ldots, \rho_N]^T$, the model of LSRMs network can be derived as,

$$\begin{bmatrix} \dot{\rho} \\ \ddot{\rho} \end{bmatrix} = \underbrace{\begin{bmatrix} 0_N & I_N \\ -\omega^2 \cdot I_N & -k_b \cdot \mathcal{L}(\mathcal{G}) \end{bmatrix}}_{\mathcal{S}} \begin{bmatrix} \rho \\ \dot{\rho} \end{bmatrix} \tag{14}$$

According to Eq. (14), the LSRMs network can be reformulated as,

$$\dot{\tilde{X}} = \mathcal{S}\tilde{X} \tag{15}$$

where $\tilde{X} = \left[\rho^T, \dot{\rho}^T\right]^T$.

To prove the LSRMs network Eq. (15) has ability to track a sinusoidal reference signal $r = M \sin(\omega t + \theta)$ without phase disparity, the following lemma is provided.

Lemma 1. *Let $\Psi_{l,i}, \Psi_{r,i}$ be the left and right eigenvectors of Laplacian matrix $\mathcal{L}$ associated to the i-th eigenvalue ψ_i, $i = 1, \ldots, N$, respectively. the eigenvalues of $\mathcal{S}$ in Eq. (15) can thus be represented as,*

$$\lambda_{i\pm} = \frac{k_b\psi_i \pm \sqrt{k_b^2\psi_i^2 - 4\omega^2}}{2},$$

and its left and right eigenvectors can be denoted as the following,

$$\Lambda_{l,i\pm} = [\Psi_{l,i}^T, \lambda_{i\pm}\Psi_{l,i}^T]^T, \Lambda_{r,i\pm} = [\Psi_{r,i}^T, -\frac{\lambda_{i\pm}}{\omega^2}\Psi_{r,i}^T]^T.$$

Proof of Lemma 1. We divide $\Lambda_{l,i\pm}, \Lambda_{r,i\pm}$ in two parts, denoted as $\Lambda_{l,i\pm} = [\Lambda_{l,u}^T, \Lambda_{l,d}^T]^T$ and $\Lambda_{r,i\pm} = [\Lambda_{r,u}^T, \Lambda_{r,d}^T]^T$, respectively. For convenience, we omit the subscript index i or $i\pm$. For $\Lambda_{l,i\pm}$, we have,

$$\begin{bmatrix} \Lambda_{l,u}^T & \Lambda_{l,d}^T \end{bmatrix} \mathcal{S} = \lambda \begin{bmatrix} \Lambda_{l,u}^T & \Lambda_{l,d}^T \end{bmatrix} \tag{16}$$

Similarly, for $\Lambda_{r,i\pm}$, we have,

$$\mathcal{S} \begin{bmatrix} \Lambda_{r,u} \\ \Lambda_{r,d} \end{bmatrix} = \lambda \begin{bmatrix} \Lambda_{r,u} \\ \Lambda_{r,d} \end{bmatrix} \tag{17}$$

From Eq.(14), Eq.(16) can be derived as,

$$\Lambda_{l,d}^T = -\frac{\lambda}{\omega^2} \cdot \Lambda_{l,u}^T \tag{18a}$$

$$\Lambda_{l,u}^T - k_b\Lambda_{l,d}^T \cdot \mathcal{L} = \lambda \cdot \Lambda_{l,d}^T \tag{18b}$$

Likewise, we can obtain the equation as,

$$\Lambda_{r,d} = \lambda \cdot \Lambda_{r,u} \tag{19a}$$

$$-\omega^2 \cdot \Lambda_{r,u} - k_b \cdot \mathcal{L}\Lambda_{r,d} = \lambda \cdot \Lambda_{r,d} \tag{19b}$$

Substituting Eq. (18a) into Eq. (18b), we obtain

$$\Lambda_{l,u}^T + \frac{k_b}{\omega^2}\lambda \cdot \Lambda_{l,u}^T \cdot \mathcal{L} = -\frac{\lambda^2}{\omega^2} \cdot \Lambda_{l,u}^T \tag{20}$$

Preprints (www.preprints.org) | NOT PEER-REVIEWED | Posted: 25 May 2017 doi:10.20944/preprints201705.0181.v1

Peer-reviewed version available at Energies 2017, 10, 949; doi:10.3390/en10070949

$$-\Lambda_{l,u}^T \cdot \mathcal{L} = \frac{\lambda^2+\omega^2}{k_b\lambda}\Lambda_{l,u}^T$$

In addition, substituting Eq. (19a) into Eq. (19b), we have

$$-\omega^2 \cdot \Lambda_{r,u} - k_b\lambda \cdot \mathcal{L} \cdot \Lambda_{r,u} = \lambda^2 \cdot \Lambda_{r,u} \tag{21a}$$

$$-\mathcal{L} \cdot \Lambda_{r,u} = \frac{\lambda^2+\omega^2}{k_b\lambda} \cdot \Lambda_{r,u} \tag{21b}$$

According to Eq. (21b), we notice $\psi = -\frac{\lambda^2+\omega^2}{k_b\lambda}$, $\Psi_l = \Lambda_{r,u}$ are the eigenvalue and left eigenvector of Laplacian matrix $\mathcal{L}$, respectively. Therefore we have

$$\lambda^2 + k_b\psi\lambda + \omega^2 = 0 \tag{22}$$

Eq. (22) can thus be solved as

$$\lambda_\pm = \frac{k_b\psi \pm \sqrt{k_b^2\psi^2 - 4\omega^2}}{2} \tag{23}$$

Besides, from (18a) and (19a), we know $\Lambda_{l\pm} = [\Psi_l^T, -\frac{\lambda_\pm}{\omega^2}\Psi_l^T]$, $\Lambda_{r\pm} = [\Psi_r^T, \lambda_\pm\Psi_r^T]^T$. *Lemma 1* is proved. □

Theorem 1. *If graph $\mathcal{G}$ describing the coordinated network includes a directed spanning tree, and the root node can access to the reference position as sinusoidal signal $r = \sin(\omega t + \theta)$ such as shown in Fig. 3a, the LSRMs network Eq. (15) can track asymptotically the reference with zero difference-phase.*

(a) with reference (b) with virtual node

Figure 3. LSRMs network with virtual LSRM modeling reference.

Proof of Theorem 2. According to [29], for a directed graph $\mathcal{G}$ with a spanning tree in the network topology, its Laplacian matrix $-\mathcal{L}(\mathcal{G})$ has the left eigenvector $\Psi_{l,1} = \mathbf{p}_N$ and the right eigenvector $\Psi_{r,1} = \mathbf{1}_N$. They correspond to a simple zero eigenvalue $\psi_1 = 0$ of $\mathcal{L}$, and all rest of eigenvalues $\psi_i, i = 2,\ldots,N$ satisfy $\mathrm{Re}(\psi_i) < 0$, where $\mathrm{Re}(\cdot)$ is the real part of a complex number. Furthermore, $\mathbf{p}_N$ satisfies

$$\begin{aligned}&\mathbf{p}_N \geq 0\\ &\mathbf{p}_N^T\mathbf{1}_N = 1.\end{aligned} \tag{24}$$

According to *Lemma 1*, the first two eigenvalues of $\mathcal{S}$ in Eq. (15) are $\lambda_{1\pm} = \pm\jmath\omega$, $\jmath$ is the imaginary unit. Accordingly, the left eigenvector and right eigenvector are $\Lambda_{l,1\pm} = [\mathbf{p}_N^T, \pm\jmath\omega\mathbf{p}_N^T]^T$, $\Lambda_{r,1\pm} = [\mathbf{1}_N^T, \pm\frac{1}{\jmath\omega}\mathbf{1}_N^T]^T$ respectively. We have

$$\mathcal{S} = \mathcal{P}\mathcal{M}\mathcal{P} \tag{25}$$

where

$$\mathcal{P}=\left[\begin{array}{c}\Lambda_{l,1\pm},\ldots,\Lambda_{l,N\pm}\end{array}\right],\mathcal{P}^{-1}=\left[\begin{array}{c}\Lambda_{r,1\pm},\ldots,\Lambda_{r,N\pm}\end{array}\right]^{T},\mathcal{M}=\left[\begin{array}{ccc}\jmath\omega & 0 & 0_{1\times(2N-2)}\\ 0 & -\jmath\omega & 0_{1\times(2N-2)}\\ 0_{(2N-2)\times 1} & 0_{(2N-2)\times 1} & J(\lambda_k)\end{array}\right]$$

Here $J(\lambda_k)$ is the Jordan block matrix associated to $k=2\pm,\ldots,N\pm$.

Since $e^{\mathcal{S}t}=\mathcal{P}e^{\mathcal{M}t}\mathcal{P}^{-1}$, $\lim_{t\to\infty}J(\lambda_k)=0_{(2N-2)\times(2N-2)}$, it follows that,

$$\begin{aligned}\lim_{t\to\infty}e^{\mathcal{S}t}=&[\Lambda_{l,1+}^T,\Lambda_{l,1-}^T]e^{\mathcal{M}_{1\pm}t}[\Lambda_{r,1+}^T,\Lambda_{r,1-}^T]\\ =&\frac{1}{2}e^{\jmath\omega t}\left[\begin{array}{c}\mathbf{1}_N\\ \jmath\omega\cdot\mathbf{1}_N\end{array}\right]\left[\begin{array}{c}\mathbf{p}_N\\ \frac{1}{\jmath\omega}\mathbf{p}_N\end{array}\right]^T+\frac{1}{2}e^{-\jmath\omega t}\left[\begin{array}{c}\mathbf{1}_N\\ -\jmath\omega\cdot\mathbf{1}_N\end{array}\right]\left[\begin{array}{c}\mathbf{p}_N\\ \frac{-1}{\jmath\omega}\mathbf{p}_N\end{array}\right]^T\\ =&\frac{[\cos(\omega t)+\jmath\sin(\omega t)]}{2}\left[\begin{array}{c}\mathbf{1}_N\\ \jmath\omega\cdot\mathbf{1}_N\end{array}\right]\left[\begin{array}{c}\mathbf{p}_N\\ \frac{1}{\jmath\omega}\mathbf{p}_N\end{array}\right]^T\\ &+\frac{[\cos(-\omega t)+\jmath\sin(-\omega t)]}{2}\left[\begin{array}{c}\mathbf{1}_N\\ -\jmath\omega\cdot\mathbf{1}_N\end{array}\right]\left[\begin{array}{c}\mathbf{p}_N\\ \frac{-1}{\jmath\omega}\mathbf{p}_N\end{array}\right]^T\\ =&\left[\begin{array}{cc}\frac{\cos(\omega t)+\jmath\sin(\omega t)}{2} & \frac{\cos(\omega t)+\jmath\sin(\omega t)}{2\omega\jmath}\\ \frac{\omega\jmath[\cos(\omega t)+\jmath\sin(\omega t)]}{2} & \frac{\cos(\omega t)+\jmath\sin(\omega t)}{2}\end{array}\right]\otimes\mathbf{1}_N\mathbf{p}_N^T\\ &+\left[\begin{array}{cc}\frac{\cos(\omega t)-\jmath\sin(\omega t)}{2} & \frac{-\cos(\omega t)+\jmath\sin(\omega t)}{2\omega\jmath}\\ \frac{\omega\jmath[-\cos(\omega t)+\jmath\sin(\omega t)]}{2} & \frac{\cos(\omega t)-\jmath\sin(\omega t)}{2}\end{array}\right]\otimes\mathbf{1}_N\mathbf{p}_N^T\\ =&\left[\begin{array}{cc}\cos(\omega t) & \frac{1}{\omega}\sin(\omega t)\\ -\omega\sin(\omega t) & \cos(\omega t)\end{array}\right]\otimes\mathbf{1}_N\mathbf{p}_N^T\end{aligned}\tag{26}$$

where $\mathcal{M}_{1\pm}=\begin{bmatrix}\omega\jmath & 0\\ 0 & -\omega\jmath\end{bmatrix}$ is a block matrix of $\mathcal{M}$ asscciated to $\lambda_{1\pm}=\pm\omega\jmath$ and the simple zero eigenvalue of $-\mathcal{L}$.

Let $\tilde{X}=\left[\rho^T,\dot{\rho}^T\right]^T$, the solution of LSRMs network in Eq. (14) can be obtained as

$$\tilde{X}(t)=e^{\mathcal{S}t}\tilde{X}(0)\tag{27}$$

Moreover, according to Eq. (26) ,

$$\begin{aligned}\lim_{t\to\infty}\tilde{X}(t)=&\lim_{t\to\infty}e^{\mathcal{S}t}\cdot\tilde{X}(0)\\ =&\left\{\left[\begin{array}{cc}\cos(\omega t) & \frac{1}{\omega}\sin(\omega t)\\ -\omega\sin(\omega t) & \cos(\omega t)\end{array}\right]\otimes\mathbf{1}_N\mathbf{p}_N^T\right\}\tilde{X}(0)\\ =&\left\{\left[\begin{array}{cc}\cos(\omega t) & \frac{1}{\omega}\sin(\omega t)\\ -\omega\sin(\omega t) & \cos(\omega t)\end{array}\right]\otimes\mathbf{1}_N\right\}\cdot\left[\mathbf{1}_2\otimes\mathbf{p}_N^T\right]\tilde{X}(0)\end{aligned}\tag{28}$$

According to Eq. (24), it can be seen that $\mathbf{p}_N$ can be set as $[1,\mathbf{0}_{N-1}^T]^T$ in Eq. (28). Therefore, Eq. (28) is derived as

$$\lim_{t\to\infty}\tilde{X}(t)=\left\{\left[\begin{array}{cc}\cos(\omega t) & \frac{1}{\omega}\sin(\omega t)\\ -\omega\sin(\omega t) & \cos(\omega t)\end{array}\right]\otimes\mathbf{1}_N\right\}x_1(0)\tag{29}$$

where $x_1(0)$ is the initial values of the LSRM node L_1 as the root of a directed spanning tree in the coordinated network topology $\mathcal{G}$, as shown in Fig. 1. In addition, the states of LSRM nodes $L_i, i = 2, \ldots, N$ converge to the steady state as,

$$\begin{cases} \rho_i(t) = \cos(\omega t)\rho_1(0) + \frac{1}{\omega}\sin(\omega t)\dot{\rho}_1(0) \\ \dot{\rho}_i(t) = -\omega\sin(\omega t)\rho_1(0) + \cos(\omega t)\dot{\rho}_1(0) \end{cases} \tag{30}$$

Obviously, the steady state values are determined by the initial values $[\rho_1(0), \dot{\rho}_1(0)]$ of root node L_1. Therefore, the states of other $N-1$ LSRM nodes $L_i, i = 2, \ldots, N$ converge to the state of root without phase disparity. The fact verifies under the effect of the coordinated control Eq. (12), the states of LSRMs network can track the state of root node L_1 represented as

$$\begin{cases} \rho_1(t) = \cos(\omega t)\rho_1(0) + \frac{1}{\omega}\sin(\omega t)\dot{\rho}_1(0) \\ \dot{\rho}_1(t) = -\omega\sin(\omega t)\rho_1(0) + \cos(\omega t)\dot{\rho}_1(0) \end{cases} \tag{31}$$

Let $\sin\theta = \rho_1(0), \cos\theta = \frac{1}{\omega}\dot{\rho}_1(0)$, Eq. (31) is rewritten as,

$$\begin{cases} \rho_1(t) = \sin(\omega t + \theta) \\ \dot{\rho}_1(t) = \omega\cos(\omega t + \theta) \end{cases} \tag{32}$$

Accordingly, if the reference sinusoidal position signal $r = \sin(\omega t + \theta)$ in Fig. 3a and its derivative is regarded as the state $[\rho_r, \dot{\rho}_r]^T$ of a virtual root node L_r, as shown in Fig. 3b, the sinusoidal reference signal can be tracked asymptotically by the LSRMs network Eq. (15) in a coupled harmonic oscillators synchronization manner . *Theorem 2* is proved. □

Remark 1. *By selecting appropriate initial values of virtual root node L_r, the LSRMs network Eq. (15) can converge to the specified sinusoidal reference, which has phase $\theta = \arcsin(\rho_r(0))$ and angular frequency $\omega = \frac{\dot{\rho}_r(0)}{\cos\theta}$.*

4. Illustrative examples

Example 1. *The sinusoidal reference r is modeled as a virtual LSRM node L_r, and its initial phase and amplitude are $\frac{\pi}{2}, 30mm$, respectively. In addition, the angular frequency of L_r is set as 2π to investigate the system control feature tracking a higher frequency sine signal.*

Each LSRM can be characterized by the second-order dynamics Eq. (11). According to the method proposed in [8], system matrices A_i and B_i $(i = 1, 2, 3)$ can be obtained by the online least squares identification [4] with a sampling time of T = 0.001 s and they can be derived as

$$A_i = \begin{bmatrix} 0 & 1 \\ 0 & 0.3333 \end{bmatrix}, B_i = \begin{bmatrix} 0 \\ 0.6667 \end{bmatrix}.$$

The initial positions of three LSRM nodes are set as $\rho_1(0) = 0, \rho_2(0) = 0, \rho_3(0) = -12$, respectively, and all velocities of three LSRM nodes are 0. The control gain k_b is set as 0.25 empirically (according to some parameter tuning experience). The topology of the LSRMs network is depicted as Fig. 3.

The results of the state and position error responses are depicted in Figs. 4a and b, respectively. Fig. 4a illustrates that the LSRMs network Eq. (14) tracks the reference $r = \sin(2\pi t + \frac{\pi}{2})$ in a zero phase-difference and asymptotic manner by applying the proposed control law Eq. (12). the position error among all nodes including $\{L_r, L_1, L_2, L_3\}$ are illustated in Fig. 4b. The disparity of position

Preprints (www.preprints.org) | NOT PEER-REVIEWED | Posted: 25 May 2017 doi:10.20944/preprints201705.0181.v1

Peer-reviewed version available at Energies 2017, 10, 949; doi:10.3390/en10070949

errors are eliminated for all LSRM nodes after about 0.9s.

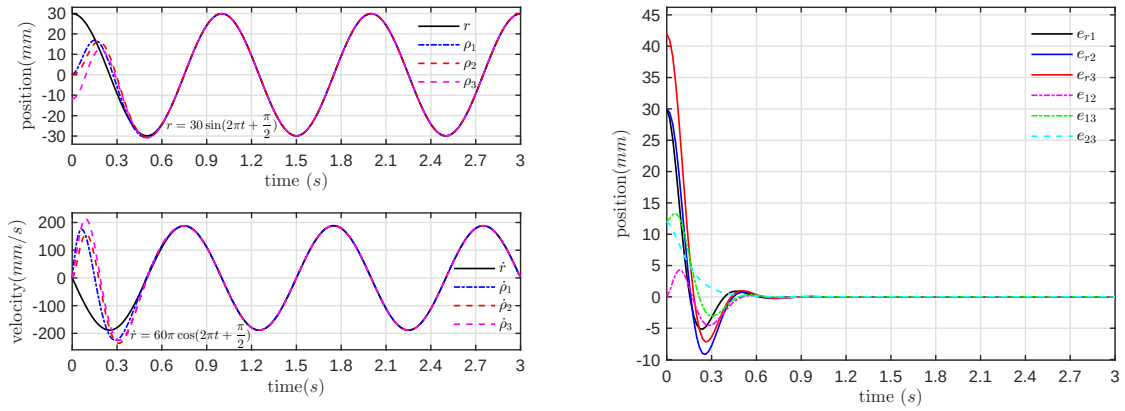

(a) (b)

Figure 4. (a) Position and velocity response and (b) relative position error response.

Example 2. *To further verify the effectiveness of the proposed control strategy, a comparative study with Example 1 are addressed. We locate the initial positions of three LSRM nodes at* $\rho_1(0) = 0, \rho_2(0) = 0, \rho_3(0) = 12$, *respectively, and three LSRM nodes start work from static state. we set the reference r initial phase as* $\frac{\pi}{2}$, *and the angular frequency are selected as* $\frac{\pi}{4}$ *to test the track feature to a lower frequency sine wave. The other systems parameters, such as the control gain etc., are given the identical values as in Example 1.*

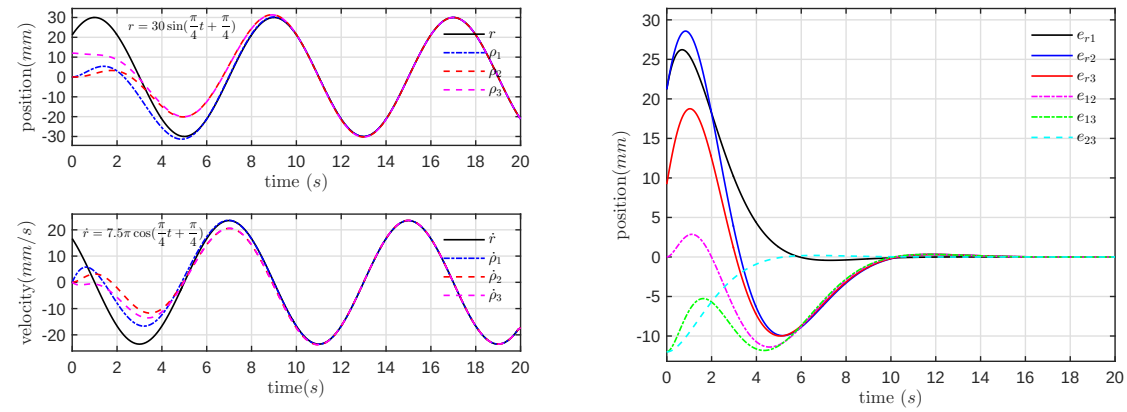

(a) (b)

Figure 5. (a) Position and velocity response and (b) relative position error response.

The simulation results are shown in Figs. 5a and b, respectively. The control performance from the proposed control method shows that a slower dynamic response can be achieved with a lower frequency sinusoidal reference, compared to Example 1 for the same system without considering uncertain parameters and external disturbances. The results also demonstrate that the LSRMs network has successfully achieved the stable state without phase-difference after 10s. Therefore, the proposed tracking control scheme has certain superior stability.

Remark 2. *From two example comparative results, it is noted that the response effectiveness of Example 2 is counterintuitive, since the state consensus process of Example 2 takes longer time rather than Example 1 as with expected. The main cause is that the angular frequency of the reference sinusoidal signal strongly effects the response rate of each LSRM node through Eq. (12).*

5. System Construction and Experimental results

5.1. System Construction

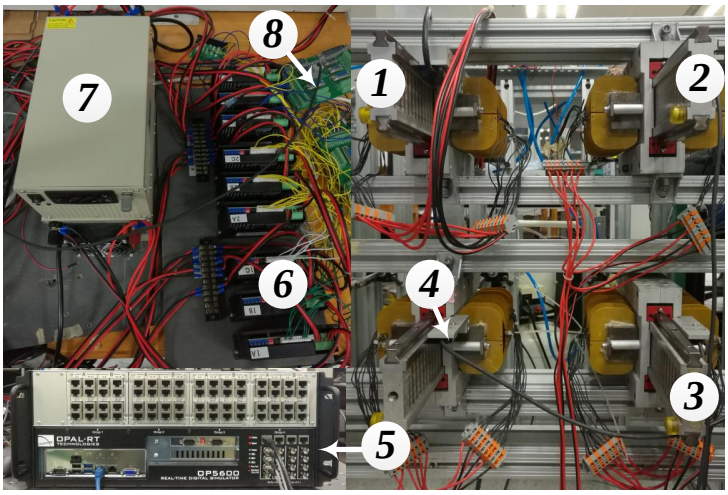

Figure 6. Experimental platform of LSRMs network. (1) LSRM 1, (2) LSRM 2, (3) LSRM 3, (4) Linear encoder, (5) RT-LAB, (6) Current amplifier, (7) Power supply, (8) Connection interface to RT-LAB

The experimental platform on the LSRMs network is exhibited in Fig. 6. The platform applies RT-LAB (OP5600) real-time digital simulator as the distributed controllers on each LSRM node, and builds a virtual LSRM node L_r modeling the specific sinusoidal reference r. The position state of each LSRM node is measured and collected by a linear magnetic encoder and inspected by the host PC which is the management terminal remotely. The sampling frequency of the position control loop is 1 kHz. The current drivers of each LSRMs node are connected to RT-LAB through the analog-to-digital converters. The current control is realized by three commercial amplifiers that are capable of inner current regulation based on the proportional-integral-differential algorithm with a switching frequency of 20 kHz. The sampling frequency of the position control loop is 1 kHz. The proposed distributed tracking control algorithm Eq. (12) can be programmed under MATLAB/Simulink® environment, and the developed algorithm can be downloaded to the digital signal processor of RT-LAB. All control parameters can be modified on-line The real time state response waveforms of all LSRM nodes of the LSRMs network are monitored and recorded by the host PC.

The control objects of three LSRM nodes are three identical LSRMs that conform to the 6/4 switched reluctance machine structure. A double-sided machine arrangement guarantees a more stable and reliable output performance and the asymmetry of the stators ensures a higher force-to-volume ratio. The major specifications of the LSRM are demonstrated in [28]. LSRM parameters can be obtained as $a_1 = 0.3, a_2 = 0.315, b_0 = 0.026, b_1 = 0.014$, and through the online recursive least square parameter identification scheme.

5.2. Experimental Results

In order to validate the proposed control scheme based on coupled harmonic oscillators, the experiment of the tracking control is implemented for the LSRMs network based on the designed controller. Moreover, to compare with two aforementioned simulation example, system scenario and

Preprints (www.preprints.org) | NOT PEER-REVIEWED | Posted: 25 May 2017 doi:10.20944/preprints201705.0181.v1

Peer-reviewed version available at Energies 2017, 10, 949; doi:10.3390/en10070949

its parameters, including initial states of the reference and LSRM nodes and its controller gain, are given the same values as in Example 1 and 2.

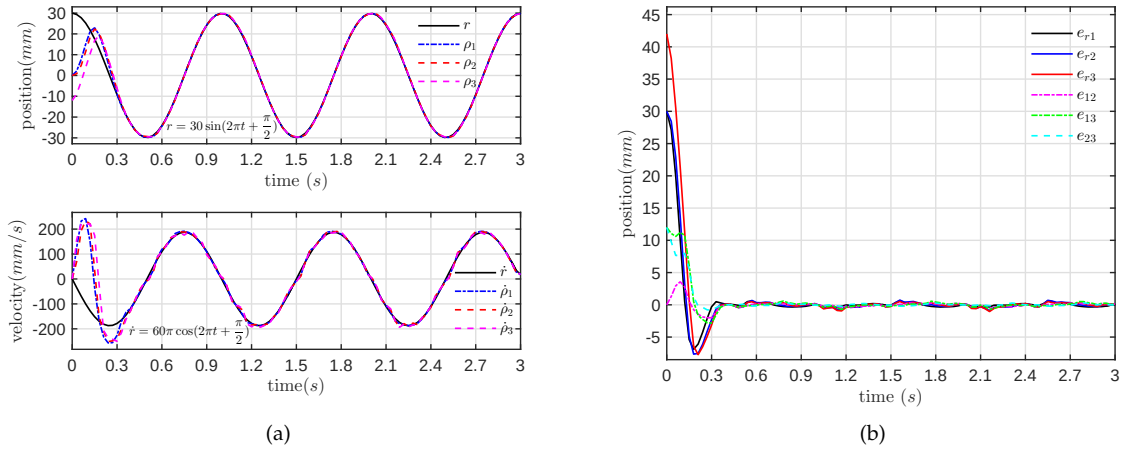

(a) (b)

Figure 7. Position and velocity of reference and three LSRMs corresponding with Example 1.

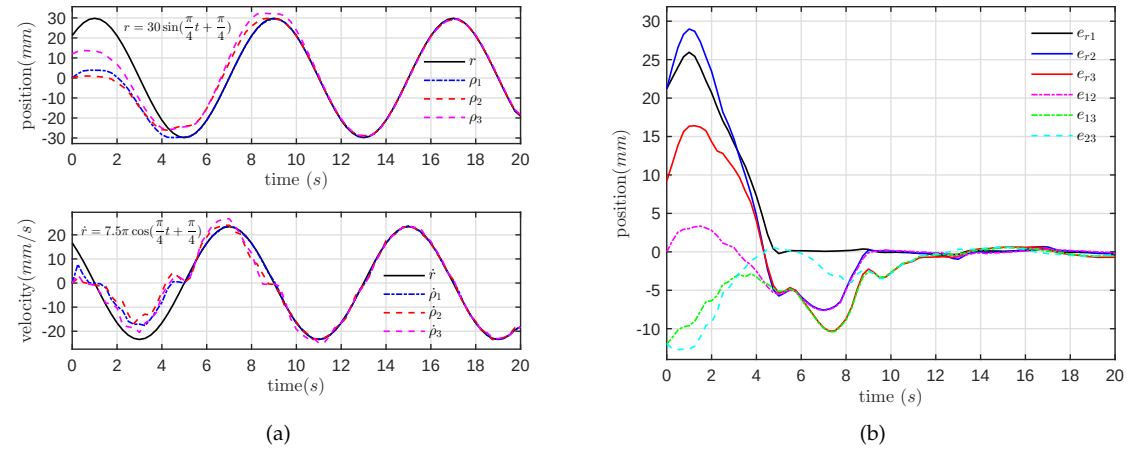

(a) (b)

Figure 8. Position and velocity of reference and three LSRMs corresponding with Example 2.

The tracking response waveforms for the three LSRMs node are shown in Fig. 7 and Fig. 8.

Fig. 7a illustrates the tracking control of three LSRM nodes takes the zero phase-difference effect at about the time of 0.4s. From Fig. 7b, the relative position errors among three LSRMs and the reference fall into 1.2mm in stable state after the transient time of 0.4s.

Fig. 8a illustrates the dynamic position and relative position error response waveforms under tracking control of three LSRM nodes. It is clear that the zero phase-difference effect is taken at about the time of 11s. From the dynamic error response profiles as Fig. 8b, it is clear that the maximum error values fall into 1.2mm.

According to the tracking profiles of the three LSRMs in Fig. 7 and Fig. 8, the LSRMs network has all capable of following the position reference signal in zero phase-difference manner. However, the control performance from the three LSRMs is disagreement and fluctuating slightly, especially at steady state. This is mainly because the imperfect manufacture and assembly of three LSRMs, which results in the asymmetric control performance from the positive and negative transitions. But from Figs. 4-5 and Figs. 7-8, it can be seen that the tracking control effect displays high similarity to the

aforementioned numerical simulative examples. It can be concluded that proposed control method is effective.

6. Conclusions

A distributed control strategy of the LSRMs network is proposed for tracking to a sinusoidal reference in a zero phase-difference manner. The dynamics of the LSRM nodes are modeled as general second-order linear systems by online system identification. Subsequently, inspired by the coupled harmonic oscillators synchronization, a distributed control is presented to track a sinusoidal reference without the phase-difference among each LSRM and the reference. Simulation and experimental results verify that the proposed control improves the synchronization and tracking accuracy performance of the LSRMs network through eliminating the phase-difference among LSRM nodes and virtual node modeling the sinusoidal reference. To further improve the tracking precision, it is suggested that the advanced internal model compensation schemes are introduced to the feedback control design of the LSRMs network. For the tracking control of some general periodical reference signals, the combined frequency domain analysis is also recommended for better control schemes.

Acknowledgments: This work was supported in part by the National Natural Science Foundation of China under Grant 51577121, 11572248, 51477103, 61690211 and 61403258.The authors also would like to thank Guangdong and Shenzhen Government under the code of S2014A030313564, 2015A010106017, 2016KZDXM007 and JCYJ20160308104825040 for support.

Author Contributions: Bo Zhang and Jianping Yuan conceived and wrote the paper main body and designed the main body of study. J.F. Pan and Li Qiu guide the system designed, analyzed the data and revised the manuscript. Wufeng Rao performed the simulations and experiments. Jianjun Luo and Honghua Dai helped to revise the paper.

Conflicts of Interest: The authors declare no conflict of interest.

Bibliography

1. Leitao, P.; Marik, V.; Vrba, P. Past, Present, and Future of Industrial Agent Applications. *IEEE Transactions on Industrial Informatics* **2013**, *9*, 2360–2372.
2. Qin, J.; Yu, C.; Gao, H. Coordination for Linear Multiagent Systems With Dynamic Interaction Topology in the Leader-Following Framework. *IEEE Transactions on Industrial Electronics* **2014**, *61*, 2412–2422.
3. Amoros, J.; Andrada, P. Sensitivity Analysis of Geometrical Parameters on a Double-Sided Linear Switched Reluctance Motor. *IEEE Transactions on Industrial Electronics* **2010**, *57*, 311–319.
4. Pan, J.F.; Zou, Y.; Cao, G. Adaptive controller for the double-sided linear switched reluctance motor based on the nonlinear inductance modelling. *Iet Electric Power Applications* **2013**, *7*, 1–15.
5. Lin, J.; Cheng, K.W.E.; Zhang, Z.; Cheung, N.C.; Xue, X.D.; Ng, T.W. Active Suspension System Based on Linear Switched Reluctance Actuator and Control Schemes. *IEEE Transactions on Vehicular Technology* **2013**, *62*, 562–572.
6. Lin, J.; Cheng, K.W.E.; Zhang, Z.; Cheung, N.C.; Xue, X.D. Adaptive sliding mode technique-based electromagnetic suspension system with linear switched reluctance actuator. *Iet Electric Power Applications* **2015**, *9*, 50–59.
7. Zhao, S.; Cheung, N.C.; Gan, W.; Yang, J.M.; Zhong, Q. Passivity-based control of linear switched reluctance motors with robustness consideration. *Iet Electric Power Applications* **2008**, *2*, 164–171.
8. Zhang, B.; Yuan, J.; Qiu, L.; Cheung, N.; Pan, J.F. Distributed Coordinated Motion Tracking of the Linear Switched Reluctance Machine-Based Group Control System. *IEEE Transactions on Industrial Electronics* **2016**, *63*, 1480–1489.
9. Qiu, L.; Shi, Y.; Pan, J.; Zhang, B.; Xu, G. Collaborative Tracking Control of Dual Linear Switched Reluctance Machines Over Communication Network With Time Delays. *IEEE Transactions on Systems, Man, and Cybernetics* **2016**, pp. 1–11.
10. Olfati-Saber, R.; Fax, J.A.; Murray, R.M. Consensus and Cooperation in Networked Multi-Agent Systems. *Proceedings of the IEEE* **2007**, *95*, 215–233.

11. Cao, Y.; Yu, W.; Ren, W.; Chen, G. An Overview of Recent Progress in the Study of Distributed Multi-Agent Coordination. *IEEE Transactions on Industrial Informatics* **2012**, *9*, 427–438.
12. Li, L.; Ho, D.W.C.; Lu, J. A Unified Approach to Practical Consensus with Quantized Data and Time Delay. *IEEE Transactions on Circuits and Systems I Regular Papers* **2013**, *60*, 2668–2678.
13. Yu, W.; Chen, G.; Cao, M.; Ren, W. Delay-Induced Consensus and Quasi-Consensus in Multi-Agent Dynamical Systems. *IEEE Transactions on Circuits and Systems I-regular Papers* **2013**, *60*, 2679–2687.
14. Wei, J.; Fang, H. Multi-agent consensus with time-varying delays and switching topologies. *Journal of Systems Engineering and Electronics* **2014**, *25*, 489–495.
15. Wang, H. Consensus of Networked Mechanical Systems With Communication Delays: A Unified Framework. *IEEE Transactions on Automatic Control* **2014**, *59*, 1571–1576.
16. Liu, K.; Zhu, H.; Lu, J. Bridging the Gap Between Transmission Noise and Sampled Data for Robust Consensus of Multi-Agent Systems. *IEEE Transactions on Circuits and Systems I-regular Papers* **2015**, *62*, 1836–1844.
17. Ning, X.; Yuan, J.; Yue, X. Uncertainty-based Optimization Algorithms in Designing Fractionated Spacecraft. *Scientific Reports* **2016**, *6*, 22979.
18. Zhang, Q.; Lapierre, L.; Xiang, X. Distributed Control of Coordinated Path Tracking for Networked Nonholonomic Mobile Vehicles. *IEEE Transactions on Industrial Informatics* **2013**, *9*, 472–484.
19. Dong, X.; Yu, B.; Shi, Z.; Zhong, Y. Time-Varying Formation Control for Unmanned Aerial Vehicles: Theories and Applications. *IEEE Transactions on Control Systems and Technology* **2014**, *23*, 340–348.
20. Cheng, M.H.; Li, Y.J.; Bakhoum, E.G. Controller Synthesis of Tracking and Synchronization for Multiaxis Motion System. *IEEE Transactions on Control Systems Technology* **2014**, *22*, 378–386.
21. Li, X.; Wang, X.; Chen, G. Pinning a complex dynamical network to its equilibrium. *Circuits and Systems I Regular Papers IEEE Transactions on* **2004**, *51*, 2074–2087.
22. Wang, X.; Su, H. Pinning control of complex networked systems: A decade after and beyond. *Annual Reviews in Control* **2014**, *38*, 103–111.
23. Cao, Y.; Ren, W. Distributed Coordinated Tracking With Reduced Interaction via a Variable Structure Approach. *IEEE Transactions on Automatic Control* **2012**, *57*, 33–48.
24. Wang, X.; Hong, Y.; Huang, J.; Jiang, Z. A Distributed Control Approach to A Robust Output Regulation Problem for Multi-Agent Linear Systems. *IEEE Transactions on Automatic Control* **2010**, *55*, 2891–2895.
25. Wieland, P.; Sepulchre, R.; Allgower, F. An internal model principle is necessary and sufficient for linear output synchronization. *Automatica* **2011**, *47*, 1068–1074.
26. Su, H.; Wang, X.; Lin, Z. Synchronization of coupled harmonic oscillators in a dynamic proximity network. *Automatica* **2009**, *45*, 2286–2291.
27. Ren, W. Synchronization of coupled harmonic oscillators with local interaction. *Automatica* **2008**, *44*, 3195–3200.
28. Pan, J.F.; Zou, Y.; Cao, G. An Asymmetric Linear Switched Reluctance Motor. *IEEE Transactions on Energy Conversion* **2013**, *28*, 444–451.
29. Mesbahi, M.; Egerstedt, M. *Graph theoretic methods in multiagent networks*; Princeton University Press, 2010; pp. 399–403.